Available online at www.sciencedirect.com
SCIENCE DIRECT®
Journal of Nuclear Materials 326 (2004) 185–194
journal of nuclear materials
www.elsevier.com/locate/jnucmat

Phase relation assessment for O–Pu–U ternary system

Shinsuke Yamanaka, Hajime Kinoshita, Ken Kurosaki *

Department of Nuclear Engineering, Graduate School of Engineering, Osaka University, Yamadaoka 2-1, Suita, Osaka 565-0871, Japan

Received 23 July 2003; accepted 9 January 2004

Abstract

The thermodynamic modelling has been performed for the O–Pu–U ternary system. In order to calculate the O–Pu–U ternary phase diagram, the interaction parameters of the excess Gibbs energies of the liquid and fluorite structure phase in the O–Pu–U system have been determined. The thermodynamic data for the liquid phase have been reassessed from the associated model in literatures to the ionic model using a least-square method. The thermodynamic data for the fluorite structure phase have been assessed using the oxygen potential data both in the hyper- and hypo-stoichiometric regions. The calculated ternary phase diagram reproduces the general features of the ternary phase diagram.

1. Introduction

Plutonium is one of the actinides formed by a neutron capture in ^{238}U during a irradiation of UO_2 in nuclear power plants. Recent technologies in the present commercial PUREX installations have made it possible to recover the plutonium efficiently from the spent nuclear fuel. Such recovered plutonium would be utilized most efficiently as metallic fuels in the fast reactors, combining with the pyro-processing for the plutonium separation [1,2]. However, since the fast reactor program is stopped, the disposition of the recovered plutonium is one of the most urgent issues at the world level for proliferation resistance [3].

Possible plutonium disposition scheme includes utilization of plutonium in the existing nuclear reactors. Various oxides, carbides, and nitrides have been studied as candidates to form either a homogeneous solid solution or a heterogeneous two-phase microstructure with the fuel [3–7]. The utilization of plutonium as mixed oxide fuel (MOX: $PuO_2 + UO_2$) is the current most practical solution for this issue since the technology for the commercial utilization of the UO_2 fuel has already been established. In addition, the very complete review on the thermophysical properties of the MOX fuel by Carbajo et al. [8] shows that various researchers have carried out intensive studies on the MOX fuel. Since the net plutonium consumption in the MOX fuel is limited, such uranium-free fuels as rock-like oxide (ROX) fuel and thorium oxide (TOX) fuel are currently investigated by various researchers [3,6,9–13] to accelerate the plutonium consumption.

Phase relation assessment for O–Pu–U system is the topic of the present study. In order to evaluate the thermodynamic properties of the oxide fuels, it is very important to understand the phase relation of the O–Pu–U system. Thermodynamic modelling was utilized for the assessment of the system based on the CALculation of PHAse Diagram (CALPHAD) technique [14], which enables us to predict not only the phase behaviour but also the thermodynamic properties in highly complex multi-component systems based on the Gibbs energy of the components. This technique has been successfully applied for such systems as O–Pu–Zr [15] and O–U–Zr [16].

In the present study, the thermodynamic modelling was carried out for the O–Pu–U system based on the data for O–Pu [15], O–U [16–20] and Pu–U [21] binary systems. In the first part of the present study, the non-ideal stoichiometric PuO_2–UO_2 pseudo-binary system

* Corresponding author. Tel.: +81-6 6879 7905; fax: +81-6 6879 7889.
E-mail address: kurosaki@nucl.eng.osaka-u.ac.jp (K. Kurosaki).

0022-3115/$ - see front matter © 2004 Elsevier B.V. All rights reserved.
doi:10.1016/j.jnucmat.2004.01.011

was assessed based on the phase diagram and heat capacity data. In the second part, the deviation from the ideal model in the non-stoichiometric fluorite structure phase was discussed with respect to the oxygen potential data. A possible ternary phase diagram for the O–Pu–U system was also calculated.

2. Calculation

2.1. Thermodynamic modelling

Thermodynamic modelling was performed using the program named POLY-3 included in Thermo-Calc [22]. The quantity stored in the data for the calculation is Gibbs energy of formation for phases, $G - H^{\mathrm{SER}}$ (J/mol), referred to a given reference state. In general, it is expressed as:

$$G - H^{\mathrm{SER}} = a + bT + cT\ln T + dT^2 + eT^3 + fT^{-1} + \cdots \quad (1)$$

where a, b, c, d, e, and f are constants, T represents temperature in Kelvin, and SER indicates 'stable element reference'. $G - H^{\mathrm{SER}}$ is given from the contribution of the enthalpy with the absolute entropy. The enthalpy has no absolute value; therefore a reference state needs to be defined. The most obvious reference state for the enthalpy is that of the element in its reference phase at 0.1 MPa and 298.15 K. In the present calculations, Eq. (1) was directly applied to the pure substances and stoichiometric compounds.

The Gibbs energy of a solid solution phase applied in the present study consists of such terms as reference (G^{ref}), ideal (G^{id}) and excess (G^{ex}) Gibbs energies as follows:

$$G = G^{\mathrm{ref}} + G^{\mathrm{id}} + G^{\mathrm{ex}}, \quad (2)$$

where G^{ref} is the contribution of pure components of the phase to the Gibbs energy, G^{id} is the ideal mixing contribution known as ideal entropy of mixing, and G^{ex} is the contribution due to non-ideal interactions between the components known as excess Gibbs energy of mixing.

These contributions, G^{ref}, G^{id}, and G^{ex} to the Gibbs energy were expressed by the general multi-sublattice model proposed by Sundman and Agren [23] in the present study. This model takes into account the preferential occupation of the atoms in the lattice that occurs when atoms are sufficiently different in size, electronegativity, or charge. As shown in Fig. 1, in a simple case of a fluorite structure (FCC_C1) phase with a formula $(A,B)_1(C)_2$, the reference (G^{ref}), ideal (G^{id}), and excess (G^{xs}) Gibbs energies are expressed as Eqs. (3)–(5), respectively.

$$G^{\mathrm{ref}} = y_A^1 y_C^2 G_{AC}^0 + y_B^1 y_C^2 G_{BC}^0, \quad (3)$$

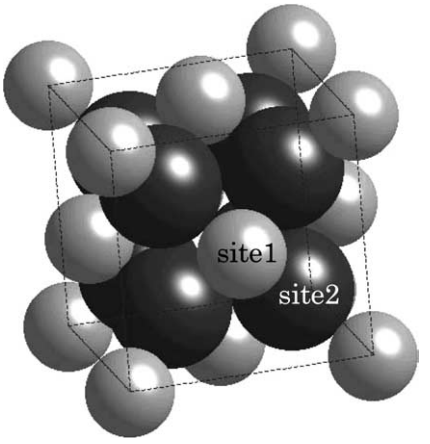

Fig. 1. Image of sublattice model for a fluorite structure phase with a formula $(A,B)_1(C)_2$: site 1 is occupied by atoms A or B; site 2 is occupied by atom C. The Gibbs energy of this solution phase is expressed based on the site fractions of $A(y_A^1)$ and $B(y_B^1)$ and the Gibbs energies of $A_1C_2(G_{AC}^0)$ and $B_1C_2(G_{BC}^0)$ using Eqs. (2)–(5).

$$G^{\mathrm{id}} = RT\{N^1(y_A^1\ln y_A^1 + y_B^1\ln y_B^1)\}, \quad (4)$$

$$G^{\mathrm{ex}} = y_A^1 y_B^1 y_C^2\{L_{A,B:C}^0 + L_{A,B:C}^1(y_A^1 - y_B^1) + L_{A,B:C}^2(y_A^1 - y_B^1)^2 + \cdots\}, \quad (5)$$

where y_i^s represents the site fraction of component 'i' on sublattice 's', G_{ij}^0 is the Gibbs energy of the pure 'ij' phase, and N^s is the total number of the site on the sublattice 's'. L_{ij}^n are constants known as interaction parameters described by using Redlich–Kister type polynomial [24].

The Redlich–Kister model is usually used to describe the excess Gibbs energy of general solutions. However, for non-metallic systems, such as oxides, an associated model [25] or an ionic liquid model [26] can be used to describe the thermodynamic properties of the liquid phase. The associated model defines as ideal reference a random mixture of atoms and associated species $(A, B, A_iB_j, \ldots)$. The ionic liquid model defines two sublattices $(A^{+a}, \ldots)_P(B^{-b}, \ldots, V^{-Q}, \ldots, A_iB_j, \ldots)_Q$, in which one is occupied by cations and the other is occupied by anions, and also there are vacancies with a negative charge Q and neutral species. P and Q are the numbers of sites on the cation and anion sublattice, respectively. P and Q are calculated from the electrical neutrality. The ionic liquid model was used to describe the liquid phase in the present study.

2.2. Phases and thermodynamic data used in the present study

The phases appear in the O–Pu–U system are α-Pu, β-Pu, γ-Pu, δ-Pu, δ′-Pu, ε-Pu (γ-U), α-U, β-U, ζ, η,

Pu_2O_3, $PuO_{1.52}$, α-$PuO_{1.61}$, PuO_{2-x} ($UO_{2\pm x}$), U_4O_9, U_3O_8, UO_3, liquid, and gas. The η phase is formed by a peritectoid reaction, $(\varepsilon\text{-Pu}, \gamma\text{-U}) + (\beta\text{-U}) = \eta$, at 70 at.%-U and 978 K. The ζ phase is formed by a peritectoid reaction, $\eta + (\beta\text{-U}) = \zeta$, at 72 at.%-U and 863 K. The sublattice models of the phases used for the calculation are summarized in Table 1.

The use of the data from different binary systems leads to the introduction of additional Gibbs energy parameters. The thermodynamic modelling of the O–Pu–U system requires thermodynamic data of its three subsystems, O–Pu, Pu–U and O–U. A set of data for the O–Pu system was obtained in our previous study [15], and the Pu–U system is also available in literature [21]. There are two different data sets for the O–U system established by Chevalier et al. [16] and Gueneau et al. [17]. The data set after Gueneau et al. has improved data of UO_{2+x} expressed by the compound energy model with ionic constituents [17]. In this model, $UO_{2\pm x}$ phase is described with three sublattices, $(U^{3+}, U^{4+}, U^{6+})_1(O^{2-}, VA)_2(O^{2-}, VA)_1$: one for cations, one for the normal site of oxygen ions and one for the interstitial oxygen ions. Vacancies are included in both oxygen sublattices. However, in the present study, the data after Chevalier et al. [16] was applied. The largest advantage of the data after Chevalier et al. is that the solid phases in the O–U system are expressed by the general multi-sublattice model, which can be readily combined with the data for O–Pu system [15] expressed by the same model.

Table 1
Phases in O–Pu–U system used in the present modelling

Phase	Sublattice model
α-Pu	$(Pu)_1$
β-Pu	$(Pu, U)_1$
γ-Pu	$(Pu, U)_1$
δ-Pu	$(Pu, U)_1(VA)_1$
δ′-Pu	$(Pu, U)_1$
ε-Pu, γ-U	$(Pu, U)_1(VA)_3$
α-U	$(Pu, U)_1$
β-U	$(Pu, U)_1$
ζ	$(Pu, U)_1$
η	$(Pu, U)_1$
Pu_2O_3	$(Pu)_2(O)_3$
$PuO_{1.52}$	$(Pu)_{100}(O)_{152}$
α-$PuO_{1.61}$	$(Pu)_{100}(O)_{161}$
PuO_{2-x}, $UO_{2\pm x}$	$(Pu, U, VA)_1(O, VA)_2$
U_4O_9	$(U)_4(O)_9$
U_3O_8	$(U)_3(O)_8$
UO_3	$(U)_1(O)_3$
Liquid	$(Pu^{4+}, U^{4+})_P(O^{2-}, VA^{Q-}, Pu_2O_3, O)_Q$ $\begin{cases} P = 2y_{Q2-} + Qy_{VA} \\ Q = 4y_{Pu4+} + 4y_{U4+} \end{cases}$
Gas	$(O_2)_1$

The Gibbs energy data used in the present calculation for the O–U, O–Pu and Pu–U binary systems are basically identical with those in literatures [15,16,21]. The Gibbs energy data for the pure substance are originated from the SGTE (Scientific Group Thermodata Europe) database [27]. The data for some of the oxides are also taken from other database [28]. The interaction parameters for the liquid phases in the O–U and Pu–U systems from literatures [16,21] were for the associated model and the general multi-sublattice model, respectively. The parameters for the liquid phase in O–U system were reassessed using a least-square method to give the same Gibbs energy curves for the ionic liquid model. That in Pu–U system was directly applicable to the ionic liquid model.

3. Results and discussion

3.1. PuO_2–UO_2 pseudo-binary system

PuO_2 and UO_2 are totally miscible in the complete composition range, because both PuO_2 and UO_2 form only a cubic (fluorite) structure phase up to their melting temperature and the ionic radii of Pu^{4+} and U^{4+} in the fluorite structure are very similar (Pu^{4+}: 0.096 nm, U^{4+}: 0.100 nm [29]). Therefore, only a fluorite structure phase and a liquid phase appear in the stoichiometric PuO_2–UO_2 pseudo-binary system.

The ideality of the PuO_2–UO_2 system is unclear. Beauvy has studied PuO_2–UO_2 solid solution and shown a possibility of its deviation from the ideality [30]. This experimental study focused on the solid solution in the low PuO_2 composition range (up to 20 mol% of PuO_2) and included the heat capacity data up to 873 K. On the other hand, Carbajo et al. has mentioned in their very completed review on the thermophysical properties of the MOX fuel that the solid solution in the PuO_2–UO_2 system is almost ideal [8]. They have also recommended that the heat capacity of the PuO_2–UO_2 solid solution should be calculated from the composition following the Neumann–Kopp rule.

Fig. 2 compares the calculated heat capacity of PuO_2, UO_2, and $(Pu_{0.25}U_{0.75})O_2$, together with the experimental data after Gibby et al. [31]. The calculation was made treating the PuO_2 and UO_2 form an ideal solid solution. The calculated and experimental values show a very good agreement. The deviation in the high temperature region is attributed to the uncertainty of the heat capacity of PuO_2. The heat capacity of PuO_2 at high temperature is not well defined. There are clear differences whether an anomalous increase occurs or not. In the present study, it is assumed that the anomalous increase does not occur.

Fig. 3(a) compares the phase diagram calculated in the present work with the recommended data for the

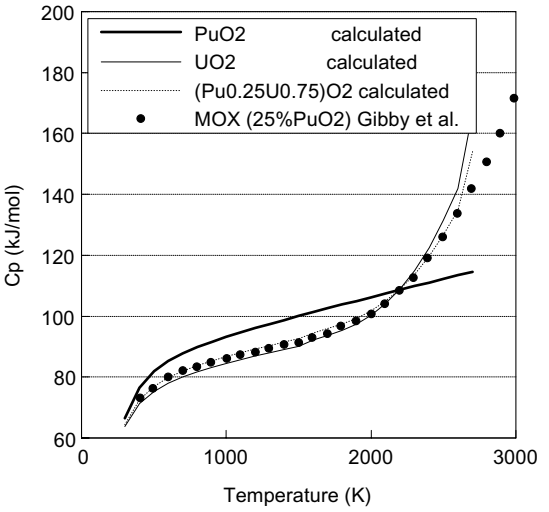

Fig. 2. Heat capacity of PuO_2, UO_2, and $(Pu_{0.25}U_{0.75})O_2$.

UO_2–PuO_2 pseudo-binary system reported in literature [8]. In this figure, the solid and dashed lines indicate the calculated results obtained in the present study and the recommended data from literature [8], respectively. Fig. 3(b) shows the experimental determined UO_2–PuO_2 pseudo-binary phase diagram reported by Lyon and Bailey [32]. Although the calculation was made treating the PuO_2 and UO_2 form ideal solid and liquid solutions, the calculated phase diagram show a very good agreement with both the recommended and experimental phase diagram even in the low PuO_2 composition range. Therefore, it is concluded that the deviation from the ideality in the stoichiometric PuO_2–UO_2 system is negligibly small.

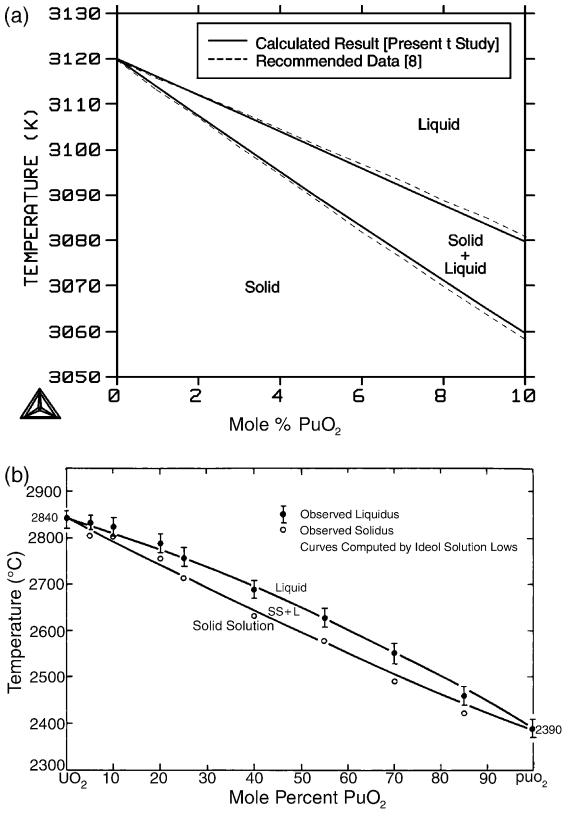

Fig. 3. (a) Phase diagram for the PuO_2–UO_2 pseudo-binary system in the low PuO_2 composition range, The solid and dashed lines indicate the calculated results obtained in the present study and the recommended data from literature [8], respectively; (b) Solid-liquid phase diagram for the PuO_2–UO_2 pseudo-binary system [32].

3.2. O–Pu–U ternary system

In the present study, we have determined the interaction parameters of the excess Gibbs energies of the liquid and fluorite structure FCC_C1 phase to calculate the O–Pu–U ternary phase diagram.

In case of the liquid phase, the interaction parameters used in the present study are summarized in Table 2. In this table, the interactions No. 1–6, which correspond to the O–Pu binary system, were derived from literature [15]. The interactions No. 7, 9, and 11, which correspond to the O–U binary system, were reassessed in the present study from the associated model in literature [16] to the ionic model using a least-square method. The interaction No. 14, which corresponds to the Pu–U binary system, was reassessed from literature data [21] by the same method as in case of the O–U binary system. Therefore, the interactions No. 8, 10, 12, 13, 15, and 16 should be additionally determined to evaluate the O–Pu–U ternary system. The interactions No. 12, 15, and 16 are not considered in this case because the P value in the sublattice model '$(Pu^{4+}, U^{4+})_P(O^{2-}, VA, Pu_2O_3, O)_Q$: $P = 2y_{O2-} + Qy_{VA}$, $Q = 4y_{Pu4+} + 4y_{U4+}$' equals zero. In addition, the parameter of the interaction No. 13 is determined as 0 because the deviation from the ideality in the UO_2–PuO_2 pseudo-binary system is negligibly small as described in the previous section. By the way, Breitung and Reil have reported the density and compressibility of liquid (U, Pu)O_2 [33]. In this paper, it is reported that the density of a solid MOX fuel is a function of the uranium and plutonium isotope vector, and the same characteristic appears to be the case in the liquid regime. Therefore, the parameters of the additional interactions No. 8 and 10 of the liquid phase are also assumed as 0.

In case of the FCC_C1 phase, the interaction parameters used in the present study are summarized in Table 3. In this table, the interaction No. 1, which corresponds to the O–Pu binary system, is derived from literature [15]. The interactions No. 2, 3, 6, and 9, which

Table 2
Values of the interaction parameters for the liquid phase: The interactions No. 8, 10, 12, 13, 15, and 16 have been determined in the present study to evaluate the O–Pu–U ternary system

No.	Interactions	Parameters	Remarks
Sublattice model: $(Pu^{4+}, U^{4+})P(O^{2-}, VA, Pu_2O_3, O)_Q$: $P = 2y_{O2-} + Qy_{VA}$, $Q = 4y_{Pu4+} + 4y_{U4+}$			
1	$L(Pu^{4+})_P(O^{2-}, VA)_Q$	0	Derived from the O–Pu binary system [15]
2	$L(Pu^{4+})_P(O^{2-}, Pu_2O_3)_Q$	$L^0_{Pu4+:O2-,Pu2O3} = +60000$ $L^1_{Pu4+:O2-,Pu2O3} = +8000$	Derived from the O–Pu binary system [15]
3	$L(Pu^{4+})_P(O^{2-}, O)_Q$	0	Derived from the O–Pu binary system [15]
4	$L(Pu^{4+})_P(VA, Pu_2O_3)_Q$	$L^0_{Pu4+:VA,Pu2O3} = +26000$ $L^1_{Pu4+:VA,Pu2O3} = +42000$ $L^2_{Pu4+:VA,Pu2O3} = -10000$	Derived from the O–Pu binary system [15]
5	$L(Pu^{4+})_P(VA, O)_Q$	0	Derived from the O–Pu binary system [15]
6	$L(Pu^{4+})_P(Pu_2O_3, O)_Q$	–	Not considered because P value equals 0
7	$L(U^{4+})_P(O^{2-}, VA)_Q$	$L^0_{U4+:O2-,VA} = +193247.68$ $L^1_{U4+:O2-,VA} = -27409.12$ $L^2_{U4+:O2-,VA} = -83302.54$	Reassessed from the associated model in the O–U binary system [16] to the ionic model
8	$L(U^{4+})_P(O^{2-}, Pu_2O_3)_Q$	0	
9	$L(U^{4+})_P(O^{2-}, O)_Q$	$L^0_{U4+:O2-,O} = -348236.67$ $L^1_{U4+:O2-,O} = +72566.67$ $L^2_{U4+:O2-,O} = +145514.33$	Reassessed from the associated model in the O–U binary system [16] to the ionic model
10	$L(U^{4+})_P(VA, Pu_2O_3)_Q$	0	
11	$L(U^{4+})_P(VA, O)_Q$	0	Reassessed from the associated model in the O–U binary system [16] to the ionic model
12	$L(U^{4+})_P(Pu_2O_3, O)_Q$	–	Not considered because P value equals 0
13	$L(Pu^{4+}, U^{4+})_P(O^{2-})_Q$	0	Determined from the UO_2–PuO_2 pseudo-binary phase diagram
14	$L(Pu^{4+}, U^{4+})_P(VA)_Q$	$L^0_{Pu4+,U4+:VA} = +4751.5681 - 12.001338T$ $L^1_{Pu4+,U4+:VA} = -2284.3112$	Reassessed from the associated model in the Pu–U binary system [21] to the ionic model
15	$L(Pu^{4+}, U^{4+})_P(Pu_2O_3)_Q$	–	Not considered because P value equals 0
16	$L(Pu^{4+}, U^{4+})_P(O)_Q$	–	Not considered because P value equals 0

correspond to the O–U binary system, are derived from literature [16]. Therefore, the interactions No. 4, 5, 7, and 8 should be additionally determined to evaluate the O–Pu–U ternary system. The additional interaction parameters have been determined by an optimization using the experimental determined oxygen potentials of MOX fuel in literatures [34–40]. In Table 3, the interaction parameters before and after optimization are listed. Figs. 4 and 5 show the calculated oxygen potentials of the MOX fuel before and after the optimization.

The modelling was performed firstly assuming all the additional interaction parameters for the fluorite structure phase as 0, and the oxygen potentials both in hyper- and hypo-stoichiometric region were calculated to compare with the experimental data available in literatures [34–40]. Fig. 4 compares the calculated oxygen potential in the fluorite structure phase in the hyper-stoichiometric region with the experimental data. At any temperatures, the values calculated before the optimizations are larger than those experimentally obtained

Table 3
Values of the interaction parameters before and after optimization for the FCC_C1 phase: The interactions No. 4, 5, 7, and 8 have been determined in the present study to evaluate the O–Pu–U ternary system

No.	Interactions	Parameters			Remarks
		Before optimization	→	After optimization	
Sublattice model: (Pu, U, VA)$_1$(O, VA)$_2$					
1	L(Pu)$_1$(O, VA)$_2$	$L^0_{\mathrm{Pu:O,VA}} = +90000 + 68T$ $L^1_{\mathrm{Pu:O,VA}} = -935000 - 196T$ $L^2_{\mathrm{Pu:O,VA}} = +787200$	→	Same as on the left	Derived from the O–Pu binary system [15]
2	L(U)$_1$(O, VA)$_2$	$L^0_{\mathrm{U:O,VA}} = +88353.17 - 32.37686T$ $L^1_{\mathrm{U:O,VA}} = +42858.36$	→	Same as on the left	Derived from the O–U binary system [16]
3	L(VA)$_1$(O, VA)$_2$	0	→	Same as on the left	Derived from the O–U binary system [16]
4	L(Pu, U)$_1$(O)$_2$	0	→	0	Determined from the UO_2–PuO_2 pseudo-binary phase diagram
5	L(Pu, VA)$_1$(O)$_2$	0	→	$L^0_{\mathrm{Pu,VA:O}} = -205000$ $L^1_{\mathrm{Pu,VA:O}} = +0$ $L^2_{\mathrm{Pu,VA:O}} = +600000$	Determined by the optimization using experimental oxygen potential potentials of MOX fuel
6	L(U, VA))$_1$(O)$_2$	$L^0_{\mathrm{U,VA:O}} = +184216.70 + 135.94271T$ $L^1_{\mathrm{U,VA:O}} = -1422742.5$ $L^2_{\mathrm{U,VA:O}} = +782551.16$	→	Same as on the left	Derived from the O–U binary system [16]
7	L(Pu, U)$_1$(VA)$_2$	0	→	$L^0_{\mathrm{Pu,U:VA}} = -340000$ $L^1_{\mathrm{Pu,U:VA}} = +1189000$ $L^2_{\mathrm{Pu,U:VA}} = -1500000$	Determined by the optimization using experimental oxygen potential potentials of MOX fuel
8	L(Pu, VA)$_1$(VA)$_2$	0	→	0	Determined by the optimization using experimental oxygen potential potentials of MOX fuel
9	L(U, VA)$_1$(VA)$_2$	0	→	Same as on the left	Derived from the O–U binary system [16]

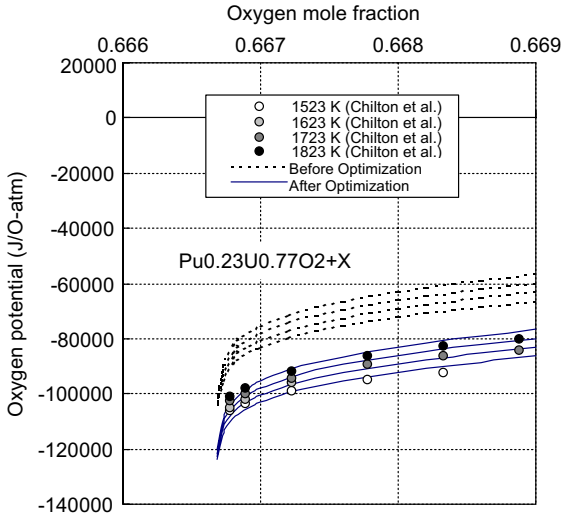

Fig. 4. Oxygen potential of fluorite structure phase in the O–Pu–U ternary phase in hyper-stoichiometric region: $Pu_{0.23}U_{0.77}O_{2+x}$.

[40]. Fig. 4 also indicates that the oxygen potential calculated using the assessed parameters and the assessed data after the optimizations, shows a very good agreement with the experimental ones.

Fig. 5 compares the oxygen potential in the fluorite structure phase but in the hypo-stoichiometric region. Similarly in the hyper-stoichiometric region, the values obtained before the optimizations differ from those experimentally obtained [34,38] in any of the compositions and temperatures. On the other hand, the values obtained after the optimizations show a very good agreement with the experimental ones. The Gibbs energy parameters for the fluorite structure phase after the optimizations are indicated in Table 4.

The ternary phase diagram for the O–Pu–U system is available in literature, as shown in Fig. 6, for the limited composition and temperature region [41]. Important features of this diagram regarding the fluorite structure phase, which is the special concern of the present study, are (i) FCC MO_{2+x} phase in U rich region becomes wider as temperature rises and (ii) FCC MO_2 + BCC MO_{2-x} region becomes much smaller as temperature rises. Using the assessed interaction parameters, ternary phase diagrams for the O–Pu–U system can be calculated. Fig. 7 shows the calculated results for both 773 and 1273 K. The tie lines in the zoomed diagrams, (b) and (d) are excluded to better visualise the phase regions. It should be noted that the FCC_C1 phase in U rich region and FCC_C1 + $PuO_{1.61}$ (BCC MO_{2-x}) regions become wider and smaller, respectively, as temperature rises, similarly to Fig. 6. We can conclude that the calculated diagrams, and therefore the assessed data,

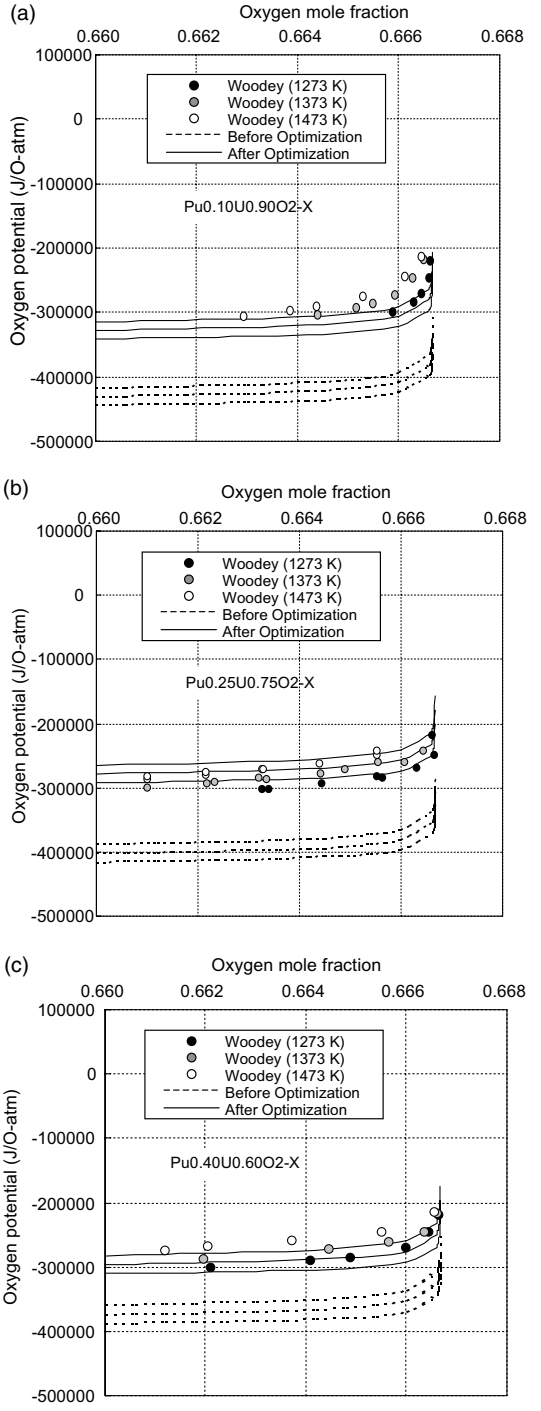

Fig. 5. Oxygen potential of fluorite structure phase in the O–Pu–U ternary phase in hyper-stoichiometric region: (a) $Pu_{0.10}U_{0.90}O_{2-x}$, (b) $Pu_{0.25}U_{0.75}O_{2-x}$ and (c) $Pu_{0.40}U_{0.60}O_{2-x}$.

reproduce the general feature of the ternary phase diagram well for 773 and 1273 K. It is noticeable that the

Table 4
Gibbs energy parameters for the fluorite structure phase used in the present modelling

Gibbs energy	Parameters (J/mol)	Temperature (K)
G_{PuO_2}	$= -1\,087\,288.7 + 505.66828T - 83.319199T\ln T - 5.8418 \times 10^{-3}T^2 - 2.2924167 \times 10^{-11}T^3 + 913\,505T^{-1}$	$298 < T < 4000$
G_{PuVA_2}	$= +42\,603.691 + 80.301382T - 18.1258T\ln T$	$298 < T < 400$
	$= -0.02241T^2 + 33\,394.038 + 236.786603T - 42.4187T\ln T$	$400 < T < 944$
	$= -0.00134493T^2 + 2.63443 \times 10^{-7}T^3 + 579\,325T^{-1} + 35\,537.844 + 232.961553T - 42.248T\ln T$	$944 < T < 4000$
G_{UO_2}	$= -1\,112\,055.29 + 433.851907T - 74.6514T\ln T - 0.00610305T^2$	$289 < T < 1500$
	$= +1.7213 \times 10^{-7}T^3 + 649\,010T^{-1} - 1\,707\,426.87 + 4369.94495T - 604.679T\ln T$	$1500 < T < 2670$
	$= +0.205276T^2 - 1.58314833 \times 10^{-5}T^3 + 126\,580\,500T^{-1} - 1\,303\,255.56 + 1218.63701T - 167.038T\ln T$	$2670 < T < 4000$
G_{UVA_2}	$= +41\,592.266 + 130.955151T - 26.9182T\ln T + 0.00125156T^2$	$298 < T < 955$
	$= -4.426050 \times 10^{-6}T^3 + 38\,568T^{-1} + 27478.2 + 292.121093T - 48.66T\ln T$	$955 < T < 4000$
G_{VAO_2}	$= +93\,038.3 - 51.0061T - 22.2720T\ln T + 0.0101978T^2 + 1.32369 \times 10^{-6}T^3 - 76\,730.0T^{-1}$	$298 < T < 1000$
	$= +86\,862.5 + 25.3198T - 33.6276T\ln T - 0.0011916T^2 + 1.35620 \times 10^{-8}T^3 + 525\,810T^{-1}$	$1000 < T < 3300$
	$= +72\,026.5 + 62.5193T - 37.9072T\ln T - 0.000850486T^2 + 2.14420 \times 10^{-8}T^3 + 8\,766\,400T^{-1}$	$3300 < T < 4000$
G_{VAVA_2}	$= +0$	$298 < T < 4000$
$L^0_{Pu:O,VA}$	$= +90\,000 + 68T$	$298 < T < 4000$
$L^1_{Pu:O,VA}$	$= -935\,000 - 196T$	$298 < T < 4000$
$L^2_{Pu:O,VA}$	$= +787\,200$	$298 < T < 4000$
$L^0_{U:O,VA}$	$= +88\,353.17 - 32.37686T$	$298 < T < 4000$
$L^1_{U:O,VA}$	$= +42\,858.36$	$298 < T < 4000$
$L^0_{VA:O,VA}$	$= +0$	$298 < T < 4000$
$L^0_{Pu,U:O}$	$= +0$	$298 < T < 4000$
$L^0_{Pu,VA:O}$	$= -205\,000$	$298 < T < 4000$
$L^1_{Pu,VA:O}$	$= +0$	$298 < T < 4000$
$L^2_{Pu,VA:O}$	$= +600\,000$	$298 < T < 4000$
$L^0_{U,VA:O}$	$= +184\,216.70 + 135.94271T$	$298 < T < 4000$
$L^1_{U,VA:O}$	$= -1\,422\,742.46$	$298 < T < 4000$
$L^2_{U,VA:O}$	$= +782\,551.16$	$298 < T < 4000$
$L^0_{Pu,U:VA}$	$= -340\,000$	$298 < T < 4000$
$L^1_{Pu,U:VA}$	$= +1\,189\,000$	$298 < T < 4000$
$L^2_{Pu,U:VA}$	$= -1\,500\,000$	$298 < T < 4000$
$L^0_{Pu,VA:VA}$	$= +0$	$298 < T < 4000$
$L^0_{U,VA:VA}$	$= +0$	$298 < T < 4000$

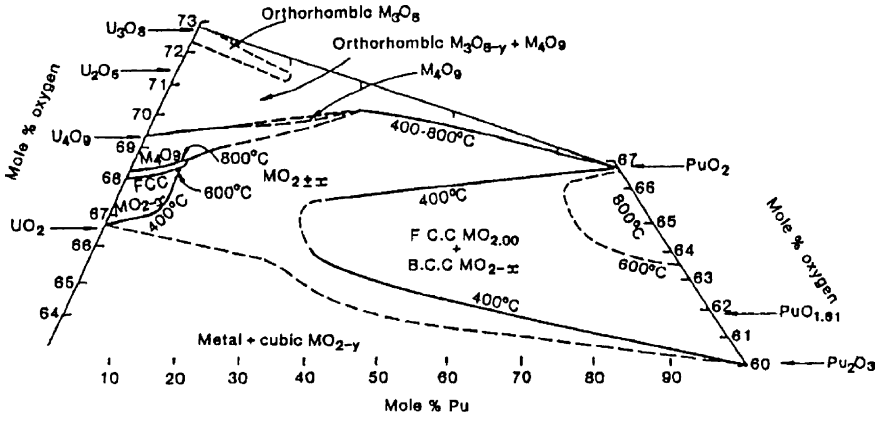

Fig. 6. Ternary phase diagram for O–Pu–U system [41].

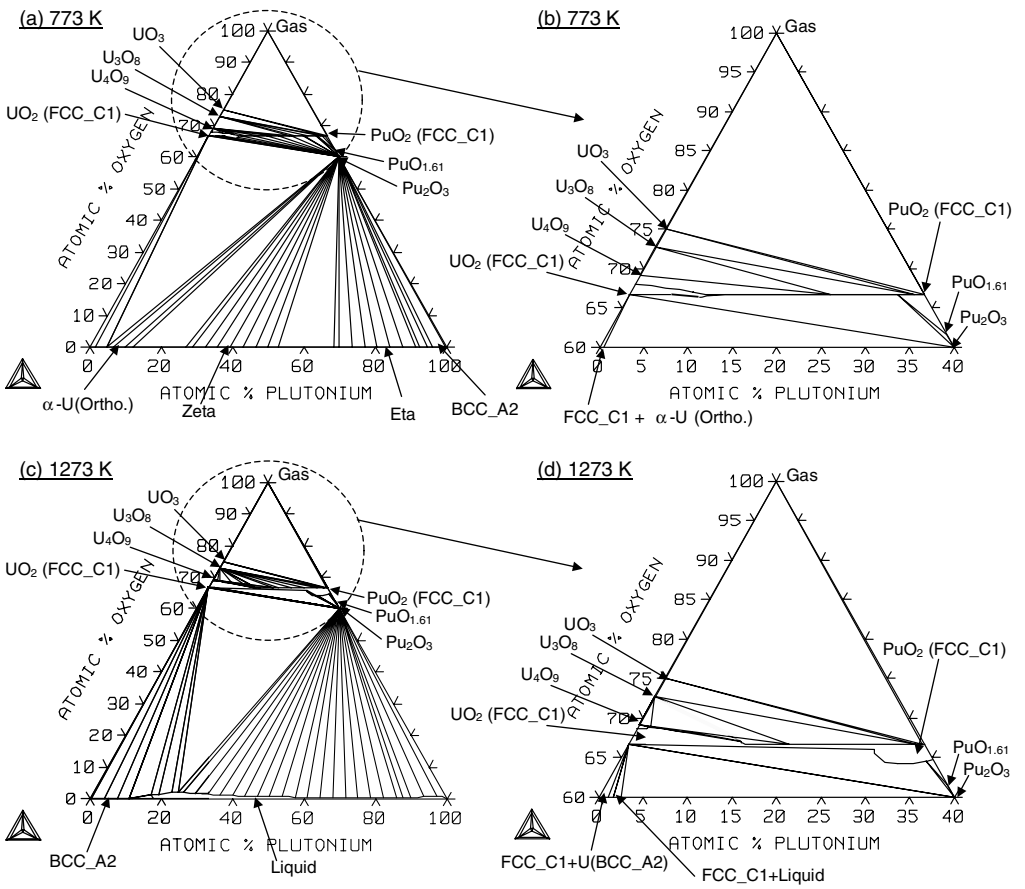

Fig. 7. Ternary phase diagram for O–Pu–U system: (a,b) 773 K zoomed in high oxygen composition region, (c,d) 1273 K zoomed in high oxygen composition region. Tie lines in the zoomed diagrams are excluded to make it easier see the phase regions.

fluorite structure (FCC_C1) phase tends to expand towards hyper- and hypo-stoichiometric direction in the U and Pu rich regions, respectively, as temperature rises.

4. Conclusion

The thermodynamic modelling was carried out for the O–Pu–U system and the deviation from the ideal

model in the fluorite structure phase was assessed based on the data for O–Pu, O–U, and Pu–U binary systems. For the stoichiometric PuO_2–UO_2 pseudo-binary system, the calculation for the heat capacity and phase diagram treating the PuO_2 and UO_2 as an ideal solid solution provides very good agreement with the experimental data available in literatures. Therefore, the deviation from the ideal model in the stoichiometric PuO_2–UO_2 system should be negligibly small. Therefore it is reasonable to treat the phases in this pseudo-binary system as ideal solutions.

For the non-stoichiometric fluorite structure phase, the thermodynamic modelling was demonstrated using the oxygen potential data. The results suggest that the data for O–Pu, O–U, and Pu–U binary systems cannot be mixed ideally to model the fluorite structure phase. The interaction parameters have been assessed, and the oxygen potential calculated using the assessed parameters shows very good agreement with the experimental ones both in hyper- and hypo-stoichiometric regions. Using the assessed interaction parameters, the ternary phase diagrams for the O–Pu–U system have been also calculated. The calculated phase diagrams reproduce the general feature of the ternary phase diagram well for 773 and 1273 K.

References

[1] T. Inoue, Prog. Nucl. Energy 40 (3–4) (2002) 547.
[2] M. Kurata, J. Nucl. Mater. 294 (2001) 123.
[3] F. Vettraino, G. Magnani, T. La Torretta, E. Marmo, S. Coelli, L. Luzzi, P. Ossi, G. Zappa, J. Nucl. Mater. 274 (1999) 23.
[4] H. Kleykamp, J. Nucl. Mater. 275 (1999) 1.
[5] W.L. Gong, W. Lutze, R.C. Ewing, J. Nucl. Mater. 277 (2000) 239.
[6] N. Nitani, T. Yamashita, T. Matsuda, S.-i. Kobayashi, T. Ohmichi, J. Nucl. Mater. 274 (1999) 15.
[7] H. Zhang, M.E. Huntelaar, R.J.M. Konings, E.H.P. Cordfunke, J. Nucl. Mater. 249 (1997) 223.
[8] J.J. Carbajo, G.L. Yoder, S.G. Popov, V.K. Ivanov, J. Nucl. Mater. 299 (2001) 181.
[9] C. Lombardi, A. Mazzola, E. Padovani, M.E. Ricotti, J. Nucl. Mater. 274 (1999) 181.
[10] T. Yamashita, N. Nitani, H. Kanazawa, M. Magara, T. Ohmichi, H. Takano, T. Muromura, J. Nucl. Mater. 274 (1999) 98.
[11] A. Shelley, H. Akie, H. Takano, H. Sekimoto, Prog. Nucl. Energy 31 (1–4) (2000) 317.
[12] T. Yamashita, H. Akie, Y. Nakano, K. Kuramoto, N. Nitani, T. Nakamura, Prog. Nucl. Energy 38 (3–4) (2001) 327.
[13] A.V. Bondarenko, O.V. Komissarov, Ya.K. Kozmenkov, Yu.V. Matveev, Yu.I. Orekhov, V.A. Pivovarov, V.N. Sharapov, J. Nucl. Mater. 319 (2003) 159.
[14] N. Saunders, A.P. Miodownik, in: CALPHAD (Calculation of Phase Diagrams): a Comprehensive Guide, Pergamon Materials Series, vol. 1, Pergamon, Oxford, UK, 1998.
[15] H. Kinoshita, M. Uno, S. Yamanaka, J. Alloys Compd. 354 (2003) 129.
[16] P.-Y. Chevalier, E. Fischer, J. Nucl. Mater. 257 (1998) 213.
[17] C. Gueneau, M. Baichi, D. Labroche, C. Chatillon, B. Sundman, J. Nucl. Mater. 304 (2002) 161.
[18] P.-Y. Chevalier, E. Fischer, B. Cheynet, J. Nucl. Mater. 303 (2002) 1.
[19] V.A. Kurepin, J. Nucl. Mater. 303 (2002) 65.
[20] Y.S. Kim, J. Nucl. Mater. 279 (2000) 173.
[21] M. Kurata, Calphad 23 (1999) 305.
[22] B. Sundman, Thermo-Calc User's Guide, Royal Institute of Technology, Sweden, 1995.
[23] B. Sundman, J. Agren, J. Phys. Chem. Solids 42 (1981) 297.
[24] O. Redlich, A.T. Kister, Ind. Eng. Chem. 40 (1948) 345.
[25] A.S. Jordan, Metall. Trans. 1 (1970) 239.
[26] M. Hillert, B. Jansson, B. Sundman, J. Agren, Metall. Trans. A 16A (1985) 261.
[27] SGTE Pure Substance Database, Edition 1998, Provided by GTT Technologies, Herzogenrath, Germany, 1998.
[28] A.T. Dinsdale, Calphad 11 (1991) 317.
[29] R.D. Shannon, Acta Crystallogr. A 32 (1976) 751.
[30] M. Beauvy, J. Nucl. Mater. 188 (1992) 232.
[31] R.L. Gibby, L. Leibowitz, J.F. Kerrisk, D.G. Clifton, J. Nucl. Mater. 50 (1974) 155.
[32] W.L. Lyon, W.E. Bailey, J. Nucl. Mater. 22 (1967) 332.
[33] W. Breitung, K.O. Reil, Nucl. Sci. Eng. 105 (1990) 205.
[34] R.E. Woodley, J. Nucl. Mater. 96 (1981) 5.
[35] T.L. Markin, E.J. McIver, in: A.E. Kay, M.B. Waldron (Eds.), Plutonium 1965, Chapman and Hall, London, 1967, p. 845.
[36] R.E. Woodley, J. Am. Ceram. Soc. 56 (3) (1973) 116.
[37] G.R. Chilton, I.A. Kirkham, in: H. Blank, R. Linder (Eds.), Plutonium 1975 and Other Actinides, Elsevier/North Holland, New York/Amsterdam, 1976, p. 171.
[38] R.E. Woodley, J. Nucl. Mater. 74 (1978) 290.
[39] R.E. Woodley, M.G. Adamson, J. Nucl. Mater. 82 (1979) 65.
[40] G.R. Chilton, J. Edwards, in: Thermodynamics of Nuclear Materials 1979, vol. I, IAEA, Vienna, 1980, p. 357.
[41] The plutonium–oxygen and uranium–plutonium–oxygen systems: a thermodynamic assessment, Technical Report Series No. 79, IAEA, Vienna, 1967.